Inorganic Chemistry
Article
Cite This: Inorg. Chem. XXXX, XXX, XXX−XXX
pubs.acs.org/IC

Extended Chemical Flexibility of Cubic Anti-Perovskite Lithium Battery Cathode Materials

Kwing To Lai,[†,‡] Iryna Antonyshyn,[†] Yurii Prots,[†] and Martin Valldor*[,†,§]

[†]Max Planck Institute for Chemical Physics of Solids, Nöthnitzer Straße 40, DE-01187 Dresden, Germany
[‡]Department of Physics, The Chinese University of Hong Kong, Shatin, Hong Kong
[§]Leibniz Institute for Solid State and Materials Research, Helmholtzstraße 20, DE-01069 Dresden, Germany

Supporting Information

ABSTRACT: Novel bichalcogenides with the general composition $(Li_2TM)ChO$ (TM = Mn, Co; Ch = S, Se) were synthesized by single-step solid-state reactions. These compounds possess cubic anti-perovskite crystal structure with $Pm\bar{3}m$ symmetry; TM and Li are disordered on the crystallographic site 3c. According to Goldschmidt tolerance factor calculations, the available space at the 3c site is too large for Li^+ and TM^{2+} ions. As cathode materials, all title compounds perform less prominent in lithium-ion battery setups in comparison to the already known TM = Fe homologue; e.g., $(Li_2Co)SO$ has a charge density of about 70 mAh g^{-1} at a low charge rate. Nevertheless, the title compounds extend the chemical flexibility of the anti-perovskites, revealing their outstanding chemical optimization potential as lithium battery cathode material.

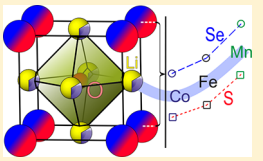

1. INTRODUCTION

The improvement of lithium battery electrode materials is challenging because of the many parameters that have to be considered: high specific charge capacity, maximum charge rate, chemical stability, safety, cost, and the environmental aspect. Simultaneously, the demand for enhanced lithium battery performance is steadily increasing because (i) petrol engines are being replaced by rechargeable batteries and (ii) alternative energy storage for solar and wind energies is necessary to bridge the energy need and availability. Of all parts in lithium batteries, primarily the cathode material requires improvements to reach higher battery energy storage capacity.[1,2] Today, we use cathode materials like olivine $Li_{1-x}FePO_4$,[3] delafossites $Li_{1-x}TMO_2$ (TM = Co,[4] Mn,[5] Ni[6]), and spinel $Li_{1+x}Mn_2O_4$.[7] The first two materials have been subjected to vast chemical substitutions in the search of more stable cathodes. In olivine, Fe can be partly or fully substituted for Mn, Co, and Ni, but the cathode performances only decrease.[3] Extended work was made on $Li_{1-x}CoPO_4$ (see, for example, ref 8); however, the working potential is too high (4.8 V vs Li^+/Li) for commercial electrolytes. Chemical alterations of the delafossites have been more successful for their performances as cathodes: the most well-known, chemically optimized compositions (commercial abbreviations) are $Li_{1-x}(Ni_{0.8}Co_{0.15}Al_{0.05})O_2$ (NCA)[9] and $Li_{1-x}(Ni_{1/3}Mn_{1/3}Co_{1/3})O_2$ (NMC).[10] According to estimations, these two compounds, together with the parent compound $LiCoO_2$, constituted a U.S. market value of about USD 20 billion in 2016.[11] Hence, improving already existing materials or finding alternative materials would be highly valued.

By chemical substitutions in the cation-vacancy-ordered anti-perovskite $(Fe_2\square)SeO$ (□ = vacancy),[12] new lithium battery cathode materials $(Li_2Fe)ChO$ (Ch = S, Se) with cubic anti-perovskite structures were discovered.[13] These materials are cheap, can be easily produced, and withstand high charging rates, making them competitive for commercial use. To make this group of materials even more attractive, it is important to widen the chemical flexibility of bichalcogenide anti-perovskites. In crystalline solid-state compounds, Fe^{2+} can usually be substituted for other transition metals, of which divalent Mn and Co have very similar coordination preferences. Here, we present the first successful and complete replacement of Fe by both Mn and Co in the cubic anti-perovskites, opening up a wide field for chemical optimizations.

2. EXPERIMENTAL DETAILS

2.1. Synthesis. All quaternaries were synthesized by the following reaction: $Li_2O + TM + Ch \rightarrow (Li_2TM)ChO$, using Li_2O (Alfa Aesar, 99.5%), TM = Mn (Alfa Aesar, 4 N) or Co (Alfa Aesar, 3 N), and Ch = S (Alfa Aesar, 99.5%) or Se (Alfa Aesar, 5 N). The constituents were mixed in an agate mortar and pressed into pellets, which were placed in corundum crucibles inside silica ampules. The ampules were melt-sealed after the inner pressure was lowered to $p < 10^{-4}$ mbar. All samples were heated up to about 750 °C at a rate of 50 °C h^{-1}. This temperature was held for 2−10 h before each ampule was quenched in water. All preparations and sample handling were done in an Ar-filled glovebox (MBraun) with O_2 and H_2O levels below 1 ppm.

2.2. X-ray Diffraction Investigations. Powder X-ray diffraction measurements were performed using Guinier cameras (Huber) equipped with an image-plate detector using a Cu $K\alpha_1$ (TM = Mn) or a Co $K\alpha_1$ (TM = Co) X-ray source. The software *JANA2006*[14] was applied to compare observed diffraction data with structural model patterns generated by the Rietveld method.

2.3. Elemental Analyses. Elemental analyses were done by inductively coupled plasma optical emission spectroscopy (ICP-OES) on a matrix-matched calibrated Vista RL spectrometer (Varian). A

Received: July 4, 2018

DOI: 10.1021/acs.inorgchem.8b01850
Inorg. Chem. XXXX, XXX, XXX−XXX

well-defined amount of each sample was dissolved in a solution of ethylenediaminetetraacetic acid (3.5 mL, 0.02 M) and an acid mixture (2.5 mL of HCl:HNO_3 = 1:1) in a turboWAVE (MLS-GmbH) at 120 °C for 15 min. All solutions were then transferred to 50 mL volumetric flasks and filled with ultrapure water.

2.4. Electrochemical Investigations. Aluminum and copper plates were used as current collectors for the cathode and anode, respectively. The slurries of each battery cathode material [(Li_2TM)-ChO; TM = Mn, Co; Ch = S, Se] and graphite (Alfa Aesar, 99.8%, ~325 mesh) anode were prepared by mixing them with carbon black (Alfa Aesar, acetylene compressed, 99.9+%, $S > A$, 75 $m^2\ g^{-1}$, bulk density 80−120 g L^{-1}) and poly(vinylidene fluoride) (Sigma-Aldrich) in mass ratio of 85:5:10 inside the organic solvent *N*-methylpyrrolidone (NMP; Sigma-Aldrich, anhydrous, 99.5%). Each slurry was homogeneously distributed on the respective metallic plate (~25 cm^2). The coated plates were treated at 100 °C for 1−2 h for the removal of organic solvent (NMP). For each trial battery assembly, ~0.3 g of active materials was used. The nonwoven separator (Freudenberg FS2226) was wetted with a mixture of 1.0 M $LiPF_6$ in ethylene carbonate (EC) and ethyl methyl carbonate (EMC) (50:50 by volume, Sigma-Aldrich) prior to placing it between the coated and dried current collectors. Each battery assembly was placed in a plastic bag with a surplus amount of electrolyte. All preparations and electrochemical measurements were performed in an Ar-filled glovebox (MBraun). The charge/discharge experiments were carried out and evaluated using a BioLogic SP300 potentiostat and *EC-Lab* (version 11.01) software, respectively.

3. RESULTS AND DISCUSSION

3.1. X-ray Diffraction Data. The obtained powders were either dark green (Mn) or dark brown (Co). Single-step syntheses result in highly crystalline materials of at least 90% purity, as estimated from powder X-ray diffraction data (Figures 1 and S1). Importantly, all samples contained fewer secondary phases (e.g., Li_2Ch and TM oxides) if the heating procedure was suddenly interrupted by quenching, i.e., by dropping the hot ampules in ice water.

The crystal structures of $(Li_2TM)ChO$ (TM = Mn, Co; Ch = S, Se) can be described as cubic anti-perovskites (Figure 2)

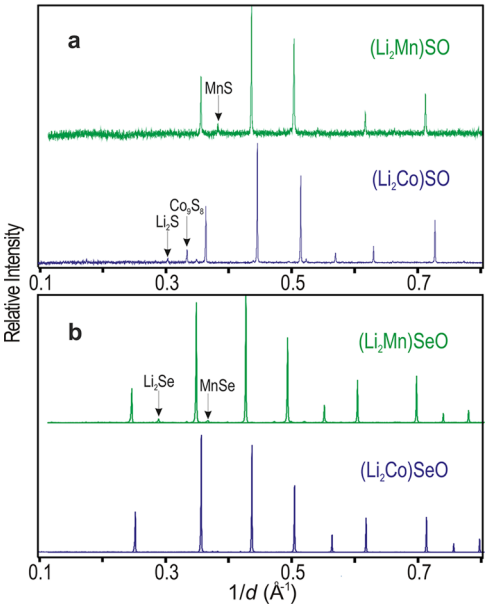

Figure 1. Powder X-ray diffraction data of (a) $(Li_2TM)SO$ and (b) $(Li_2TM)SeO$ (TM = Mn, Co). The strongest intensities of the secondary phases are marked.

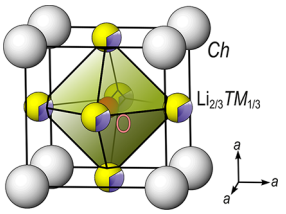

Figure 2. Unit cell content of cubic anti-perovskites $(Li_2TM)ChO$ (TM = Mn, Co; Ch = S, Se) with an emphasized octahedron around the O ion.

with the space group $Pm\bar{3}m$. Refinement details can be found in Table S1. Li^+ and TM^{2+} are randomly distributed on the same positions on the atomic lattice. On the contrary, the anions O^{2-} and Ch^{2-} are perfectly ordered in a CsCl-like manner without intermixing. As expected for an anti-perovskite structure, (Li, TM) and Ch together form a cubic close-packing where O^{2-} ions occupy octahedral voids of cations. The corresponding Niggli notation for a generalized structure is $^3_\infty[O(Li_{2/3}TM_{1/3})_{6/2}]^{2+}Ch^{2-}$, where Ch can be regarded as a guest in the Li−TM−O host network. In a comparison also with the Fe homologues, the unit cell sizes of $(Li_2TM)ChO$ (TM = Mn, Fe, Co; Ch = S, Se) increase expectedly from S to Se and from Co to Mn (Figure 3).

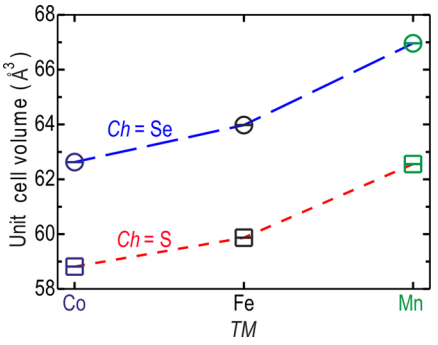

Figure 3. Unit cell volumes presented as a function of the content at the TM and Ch sites. For TM = Fe, data are taken from ref 13.

3.2. Chemical Compositions. To verify the relative atomic compositions, including electron-poor Li, ICP-OES analyses were performed, revealing that the bulk sample compositions are close to the nominal ones (Table 1). No other elements were observed in the spectroscopic data.

Table 1. ICP-OES Data of the Title Compounds[a]

starting composition	spectroscopic result
$(Li_2Mn)SO$	$Li_{1.97(1)}Mn_{1.008(5)}S_{0.98(2)}O_{1.043(4)}$
$(Li_2Co)SO$	$Li_{2.03(5)}Co_{1.02(2)}S_{1.02(1)}O_{0.933(8)}$
$(Li_2Mn)SeO$	$Li_{1.98(3)}Mn_{1.01(2)}Se_{1.001(7)}O_{1.01(1)}$
$(Li_2Co)SeO$	$Li_{1.97(2)}Co_{1.04(2)}Se_{1.05(2)}O_{0.93(1)}$

[a]The results are scaled to a sum of about 5.

In air, all as-prepared powders readily decompose into binaries (Figure S2); the more ionic character with sulfide oxides compared to selenide oxides could explain why compounds with Ch = S seem to decompose faster than those with Ch = Se. Further, compounds with TM = Mn decompose faster than those with TM = Co, which might correlate with the more negative formation enthalpy of

DOI: 10.1021/acs.inorgchem.8b01850
Inorg. Chem. XXXX, XXX, XXX−XXX

$Mn(OH)_2$ ($H_f \approx -700$ kJ mol^{-1}) compared to that of $Co(OH)_2$ ($H_f \approx -540$ kJ mol^{-1}); this agrees with the observation of $Mn(OH)_2$ in the diffraction patterns (Figure S2). Note that under inert conditions none of the prepared compounds seems to decompose at room temperature.

To get an indirect hint on the mobility of Li^+ ions in these anti-perovskites, the Goldschmidt tolerance factors (t)[15] were calculated using an average ionic radius for the Li_2TM site according to $t = \frac{r_{Ch} + r_{Li_2TM}}{\sqrt{2}(r_O + r_{Li_2TM})}$ and the ideal cubic unit cell parameter according to $a = \sqrt{2}(r_{Ch} + r_{Li_2TM})$ Å [$r(O^{2-}) = 1.26$, $r(S^{2-}) = 1.70$, and $r(Se^{2-}) = 1.84$ Å].[16] The calculated tolerance factors and ideal cubic cell parameters are much smaller than observations (Table 2). This is suggestive of relatively large voids for the cations to occupy, which is a prerequisite for extraordinary Li^+ mobility. The distance between cation sites, ~2.8 or $a/\sqrt{2}$ Å, is also similar to that in delafossites $Li_{1-x}TMO_2$ (TM = Co, Mn, Ni),[4−6] which exhibit relatively high Li^+ migration rates. Theoretical model calculations support high migration rates in cubic anti-perovskites; the Li^+ diffusion barrier in $(Li_2Fe)SO$ was estimated to be about 0.35 eV,[17] which is comparable with that of superionic Li conductors like Li_3ClO,[18] where its Li diffusion mechanism has been theoretically predicted to be driven by Li^+ partly occupying interstitial sites.[19−21]

Table 2. Goldschmidt Factors for $(Li_2TM)ChO$ (TM = Co, Mn; Ch = S, Se)

	TM, Ch			
	Mn, S	Co, S	Mn, Se	Co, Se
$r(Li_2TM)$ [Å]	0.9233	0.895	0.9233	0.895
t	0.850	0.852	0.895	0.898
ideal a [Å]	3.7093	3.6693	3.9073	3.8673
obsd a [Å]	3.9697(1)	3.8889(1)	4.0608(1)	3.97119(8)

Similar to delafossites $Li_{1-x}TMO_2$ (TM = Co,[4] Mn,[5] Ni[6]),[9,10] the cubic anti-perovskite title compounds exhibit a vast chemical diversity, forming with TM = Mn, Fe,[13] and Co. However, an important difference is that the anti-perovskites have the pristine formal oxidation state 2+ of TM, while it is 3+ in delafossites. Hence, the working potentials are relatively lower for anti-perovskite cathodes with redox pairs Mn^{2+}/Mn^{3+}, Fe^{2+}/Fe^{3+},[13] and Co^{2+}/Co^{3+}. Fortunately, all of these 2+/3+ redox pairs are found within the potential window where the standard constituents of a battery are stable. This means that the anti-perovskites can be charged/discharged with less risk for the irreversible decomposition of anode materials or electrolytes compared to high-voltage cathodes, like $Li_{1+x}Mn_2O_4$,[22] where deteriorations shorten the battery lifetime.

3.3. Electrochemical Investigations. To enable a direct comparison between the Mn- and Co-based anti-perovskites, presented here, with the previously known Fe-based ones,[13] a graphite anode was used, which notably lowers the working potential of the battery setups. According to preliminary charging/discharging experiments (Figures 4 and S3−S5), most of the materials presented here perform reasonably in a lithium battery but not as outstanding as $(Li_2Fe)ChO$ (Ch = S, Se) do. $(Li_2Co)SO$ can be reversibly cycled at low charge rates (Figure 4) with a reasonable charge capacity of ~70 mAh g^{-1} in the potential range of 1.1−2.5 V versus graphite, which proves to be a suitable potential range for all anti-perovskites.

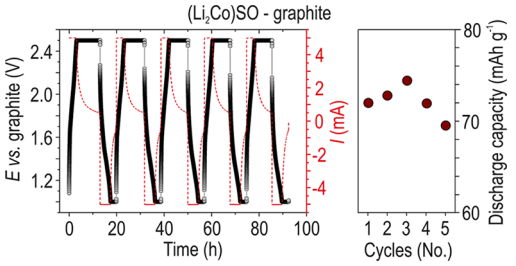

Figure 4. Five cycles of charging/discharging of a $(Li_2Co)SO$−graphite cell (left panel) with the corresponding specific discharge capacity at a charge rate of about C/15 (right panel).

Much higher charge rates up to 1.7C were tested for the battery with a $(Li_2Co)SeO$ cathode (Figure S4), revealing relatively low charge capacity (~25 mAh g^{-1}), of which 24% is lost after 100 cycles at the highest charge rate. The fact that relatively high charge rates can be used agrees with the exceedingly high Li^+ migration rates that have been reported in anti-perovskite structures.[18−21] In a wider comparison, commercial intercalation oxide cathode materials exhibit relatively higher charge densities (140−170 mAh g^{-1}) and broader working potential windows.[23] However, we anticipate that synthesized anti-perovskites with TM = Fe/Mn/Co admixtures in $(Li_2TM)SO$ are very promising for improving especially the charge density and chemical stability of this family of novel lithium battery cathode materials. For example, the solid solution $(Li_2Fe_{0.5}Mn_{0.5})SO$ might have a better cathode performance than $(Li_2Fe)SO$[13] and $(Li_2Mn)SO$ do. A similar case can be found in the delafossite solid solution $Li(Ni_{0.8}Co_{0.15}Al_{0.05})O_2$[9] with an electrode performance that surpasses those of end members $LiNiO_2$ and $LiCoO_2$.[23]

4. CONCLUSIONS

In summary, the cubic anti-perovskites $(Li_2TM)ChO$ can be synthesized by a single solid-state reaction at low temperatures and short reaction times. They exhibit an extraordinary chemical flexibility where TM can be Mn, Fe, and Co and Ch can be S and Se; their cubic unit cell parameters scale with the sizes of the involved ions, in accordance with Vegard's law. The anti-perovskites with TM = Mn or Co, presented here, perform only satisfactorily in comparison to the outstanding lithium battery cathode performance found with TM = Fe. However, these chemical extensions offer chemical optimization to synthesize solid solutions of Mn/Fe/Co at TM that might result in cathode materials for lithium-ion batteries with improved properties compared to all "end members" with TM = Mn, Fe, or Co.

■ ASSOCIATED CONTENT

Supporting Information

The Supporting Information is available free of charge on the ACS Publications website at DOI: 10.1021/acs.inorgchem.8b01850.

Powder X-ray diffraction data, crystal structure models based on Rietveld simulations, powder X-ray diffraction data of samples exposed to air, charge/discharge curves, different charge rates and discharge capacities, and $(Li_2Mn)SeO$−graphite battery (PDF)

DOI: 10.1021/acs.inorgchem.8b01850
Inorg. Chem. XXXX, XXX, XXX−XXX

AUTHOR INFORMATION

Corresponding Author

*E-mail: m.valldor@ifw-dresden.de.

ORCID

Kwing To Lai: 0000-0001-9935-202X
Iryna Antonyshyn: 0000-0002-7652-0630
Yurii Prots: 0000-0002-7418-9892
Martin Valldor: 0000-0001-7061-3492

Author Contributions

All authors have given approval to the final version of the manuscript.

Notes

The authors declare no competing financial interest.

ACKNOWLEDGMENTS

We thank Gudrun Auffermann for elemental analyses and Steffen Hückmann for powder X-ray diffraction measurements. Liu Hao Tjeng and Juri Grin are acknowledged for their support and help. This work was supported by the German Science Foundation through Projects VA 831/4-1 and SFB 1143.

REFERENCES

(1) Chu, S.; Cui, Y.; Liu, N. The path towards sustainable energy. *Nat. Mater.* **2017**, *16*, 16−22.

(2) Grey, C. P.; Tarascon, J. M. Sustainability and *in situ* monitoring in battery development. *Nat. Mater.* **2017**, *16*, 45−56.

(3) Padhi, A. K.; Najundaswamy, K. S.; Goodenough, J. B. Phospho-olivines as positive-electrode materials for rechargeable lithium batteries. *J. Electrochem. Soc.* **1997**, *144*, 1188−1194.

(4) Mizushima, K.; Jones, P. C.; Wiseman, P. J.; Goodenough, J. B. Li_xCoO_2 ($0<x \leq 1$): A new cathode material for batteries of high energy density. *Mater. Res. Bull.* **1980**, *15*, 783−789.

(5) Armstrong, A. R.; Bruce, P. G. Synthesis of layered $LiMnO_2$ as an electrode for rechargeable lithium batteries. *Nature* **1996**, *381*, 499−500.

(6) Ebner, W.; Fouchard, D.; Xie, L. The $LiNiO_2$/carbon lithium-ion battery. *Solid State Ionics* **1994**, *69*, 238−256.

(7) Thackeray, M. M.; David, W. I. F.; Bruce, P. G.; Goodenough, J. B. Lithium insertion into manganese spinels. *Mater. Res. Bull.* **1983**, *18*, 461−472.

(8) Xing, L. Y.; Hu, M.; Tang, Q.; Wei, J. P.; Qin, X.; Zhou, Z. Improved cyclic performances of $LiCoPO_4$/C cathode materials for high-cell-potential lithium-ion batteries with thiophene as an electrolyte additive. *Electrochim. Acta* **2012**, *59*, 172−178.

(9) Guilmard, M.; Croguennec, L.; Delmas, C. Thermal stability of lithium nickel oxide derivatives. Part II: $Li_xNi_{0.70}Co_{0.15}Al_{0.15}O_2$ and $Li_xNi_{0.90}Mn_{0.10}O_2$ (x = 0.50 and 0.30). Comparison with $Li_xNi_{1.02}O_2$ and $Li_xNi_{0.89}Al_{0.16}O_2$. *Chem. Mater.* **2003**, *15*, 4484−4493.

(10) Belharouak, I.; Sun, Y. − K.; Liu, J.; Amine, K. $Li(Ni_{1/3}Co_{1/3}Mn_{1/3})O_2$ as a suitable cathode for high power applications. *J. Power Sources* **2003**, *123*, 247−252.

(11) Report ID: GVR-1-68038-601-1 (2017), https://www.grandviewresearch.com/industry-analysis/lithium-ion-battery-market.

(12) Valldor, M.; Wright, T.; Fitch, A.; Prots, Yu. Metal vacancy ordering in an antiperovskite resulting in two modifications of Fe_2SeO. *Angew. Chem., Int. Ed.* **2016**, *55*, 9380−9383.

(13) Lai, K. T.; Antonyshyn, I.; Prots, Yu.; Valldor, M. Anti-perovskite Li-battery cathode materials. *J. Am. Chem. Soc.* **2017**, *139*, 9645−9649.

(14) Petříček, V.; Dušek, M.; Palatinus, L. Crystallographic computing system JANA2006: general features. *Z. Kristallogr. - Cryst. Mater.* **2014**, *229*, 345−352.

(15) Goldschmidt, V. M. Die Gesetze der Krystallochemie. *Naturwissenschaften* **1926**, *14*, 477−485.

(16) Shannon, R. D. Revised effective ionic radii and systematic studies of interatomic distances in halides and chalcogenides. *Acta Crystallogr., Sect. A: Cryst. Phys., Diffr., Theor. Gen. Crystallogr.* **1976**, *32*, 751−767.

(17) Lu, Z.; Ciucci, F. Anti-perovskite cathodes for lithium batteries. *J. Mater. Chem. A* **2018**, *6*, 5185−5192.

(18) Emly, A.; Kioupakis, E.; van der Ven, A. Phase stability and transport mechanisms in antiperovskite Li_3OCl and Li_3OBr superionic conductors. *Chem. Mater.* **2013**, *25*, 4663−4670.

(19) Mouta, R.; Melo, M. Á. B.; Diniz, E. M.; Paschoal, C. W. A. Concentration of charge carriers, migration, and stability in Li_3OCl solid electrolytes. *Chem. Mater.* **2014**, *26*, 7137−7144.

(20) Lu, Z.; Chen, C.; Baiyee, Z. M.; Chen, X.; Niu, C.; Ciucci, F. Defect chemistry and lithium transport in Li_3OCl anti-perovskite superionic conductors. *Phys. Chem. Chem. Phys.* **2015**, *17*, 32547−32555.

(21) Stegmaier, S.; Voss, J.; Reuter, K.; Luntz, A. C. Li^+ Defects in a solid-state Li ion battery: theoretical insights with a Li_3OCl electrolyte. *Chem. Mater.* **2017**, *29*, 4330−4340.

(22) Tarascon, J. M.; Guyomard, D. The $Li_{1+x}Mn_2O_4$/C rocking-chair system: A review. *Electrochim. Acta* **1993**, *38*, 1221−1231.

(23) Nitta, N.; Wu, F.; Lee, J. T.; Yushin, G. Li-ion battery materials: Present and future. *Mater. Today* **2015**, *18*, 252−264.

DOI: 10.1021/acs.inorgchem.8b01850
Inorg. Chem. XXXX, XXX, XXX−XXX